Glycine *N*-Methyltransferase Tumor Susceptibility Gene in the Benzo(*a*)pyrene-Detoxification Pathway

Shih-Yin Chen,[1] Jane-Ru Vivan Lin,[1] Ramalakshmi Darbha,[2] Pinpin Lin,[3] Tsung-Yun Liu,[4] and Yi-Ming Arthur Chen[1]

[1]*Division of Preventive Medicine, Institute of Public Health, and AIDS Prevention and Research Centre, National Yang-Ming University, Taipei, Taiwan, Republic of China;* [2]*Biomolecular Structure Section, Macromolecular Crystallography Laboratory, National Cancer Institute-Frederick, Frederick, Maryland;* [3]*Institute of Toxicology, Chung-Shan Medical University, Taichung, Taiwan, Republic of China; and* [4]*Department of Medical Research, Taipei Veterans General Hospital, Taiwan, Republic of China*

ABSTRACT

Glycine *N*-methyltransferase (GNMT) affects genetic stability by (*a*) regulating the ratio of *S*-adenosylmethionine to *S*-adenosylhomocystine and (*b*) binding to folate. Based on the identification of GNMT as a 4 S polyaromatic hydrocarbon-binding protein, we used liver cancer cell lines that expressed GNMT either transiently or stably in cDNA transfections to analyze the role of GNMT in the benzo(*a*)pyrene (BaP) detoxification pathway. Results from an indirect immunofluorescent antibody assay showed that GNMT was expressed in cell cytoplasm before BaP treatment and translocated to cell nuclei after BaP treatment. Compared with cells transfected with the vector plasmid, the number of BaP-7,8-diol 9,10-epoxide-DNA adducts that formed in GNMT-expressing cells was significantly reduced. Furthermore, the dose-dependent inhibition of BaP-7,8-diol 9,10-epoxide-DNA adduct formation by GNMT was observed in HepG2 cells infected with different multiplicities of infection of recombinant adenoviruses carrying GNMT cDNA. According to an aryl hydrocarbon hydroxylase enzyme activity assay, GNMT inhibited BaP-induced cytochrome P450 1A1 enzyme activity. Automated BaP docking using a Lamarckian genetic algorithm with GNMT X-ray crystallography revealed a BaP preference for the *S*-adenosylmethionine-binding domain of the dimeric form of GNMT, a novel finding of a cellular defense against potentially damaging exposures. In addition to GNMT, results from docking experiments showed that BaP binds readily with other DNA methyltransferases, including *Hha*I , *Hae*III, *Pvu*II methyltransferases and human DNA methyltransferase 2. We therefore hypothesized that BaP-DNA methyltransferase and BaP-GNMT interactions may contribute to carcinogenesis.

INTRODUCTION

Benzo(*a*)pyrene (BaP) is a carcinogen produced by organic material combustion. Workers in gas generation and steel plants and individuals engaged in aluminum reduction and roofing have higher cancer risks associated with long-term exposure to various polycyclic aromatic hydrocarbons including BaP (1). After diffusing into a cell, BaP binds with an aryl hydrocarbon receptor (AhR), translocates into the cell's nuclei, and transactivates the cytochrome P450 1A1 (CYP1A1) gene (2–4). A metabolic BaP product known as BaP-7,8-diol 9,10-epoxide (BPDE) is capable of forming DNA adducts and triggering mutagenesis (5).

Glycine *N*-methyltransferase (GNMT; EC2.1.1.20), a protein with multiple functions, affects genetic stability by (*a*) regulating the ratio of *S*-adenosylmethionine (SAM) to *S*-adenosylhomocystine and (*b*) binding to folate (6, 7). We have reported previously (8, 9) on diminished GNMT expression levels in both human hepatocellular carcinoma cell lines and tumor tissues. In previous projects, we localized the human GNMT gene to the 6p12 chromosomal region

and characterized its polymorphism (10, 11). Genotypic analyses of several human GNMT gene polymorphisms showed a loss of heterozygosity in 36–47% of the genetic markers in hepatocellular carcinoma tissues (11). In this study, we evaluated the effects of GNMT on liver cells treated with BaP in a transient transfection system or with stably expressed clones, based on the identification of GNMT as a 4 S polycyclic aromatic hydrocarbon-binding protein (12). We also used automated docking with a Lamarckian genetic algorithm (LGA) to elucidate GNMT-BaP interaction. In light of results showing a BaP binding preference for the SAM-binding domain of GNMT, we expanded our BaP docking experiments to include other SAM-dependent methyltransferases; our results show that BaP interacts readily with DNA methyltransferases that use cytosine as a target atom.

MATERIALS AND METHODS

Cell Lines and Culture. Two hepatocellular carcinoma cell lines [Huh7 (13) and HA22T/VGH (14)] and one human hepatoblastoma cell line [HepG2 (15)] were used in this study. Cells were cultured in DMEM (GIBCO BRL, Grand Island, NY) with 10% heat-inactivated fetal bovine serum (HyClone, Logan, UT), penicillin (100 IU/ml), streptomycin (100 μg/ml), nonessential amino acids (0.1 mM), fungizone (2.5 mg/ml), and L-glutamine (2 mM) in a humidified incubator with 5% CO_2.

Construction of pGNMT, pGNMT-antisense, and pGNMT-His-short Plasmids. To construct plasmid pGNMT containing the cytomegalovirus (CMV) promoter and GNMT cDNA fragment, we used plasmid-pFLAG-CMV-5 (Kodak, Rochester, NY) as a vector and the pBluescript-GNMT-9-1-2 phagemid (8) as the PCR template for generating the insert. A 0.9-kb DNA fragment containing the GNMT cDNA sequence and restriction enzyme sites on both ends was amplified. All PCR conditions were as recommended by the manufacturer (Perkin-Elmer, Norwalk, CT), with two exceptions (2 mM $MgCl_2$ and 150 nM primer). Twenty amplification cycles were performed using Perkin-Elmer Amplitaq Gold Taq DNA polymerase with DNA Thermal Cycler. Each PCR cycle entailed a primer annealing step at 60°C for 30 s and an extension step at 72°C for 30 s. The upstream primer (5′-gcggaattcATGGTGGACAGCGTGTAC-3′) included a 3-bp "clamp" (gcg) at the 5′ end followed by a single restriction enzyme site (*Eco*RI) and the GNMT cDNA sequence. The downstream primer (5′-gcggaattcGTCTGTCCTCTTGAG-CAC-3′) contained a similar structural motif as the upstream primer; however, it consisted of a negative strand sequence from the terminal region of the GNMT cDNA. Immediately after amplification, SDS (0.1%) and EDTA (5 mM) were added to the PCR reaction; DNA was precipitated with 2.5 M ammonium acetate and 70% ethanol. After digestion with *Eco*RI, the DNA fragment was isolated by elution from the agarose gel and ligated to *Eco*RI-digested pFLAG-CMV-5.

We used two primers (F1, 5′-gcggaattcATGGTGGACAGCGTGTAC-3; R1, 5′-gcggaattcTGTACTCGGCGGTGCGGC-3) to construct an antisense-GNMT plasmid (pGNMT-antisense) for amplifying a 136-bp DNA fragment from phagemid pBluescript-GNMT-9-1-2 (8). The fragment contained an antisense sequence spanning the GNMT translational starting site and two restriction enzyme sites (*Eco*RI and *Bam*HI) at its terminals. Cloning procedures were similar to those described for pGNMT.

To express the GNMT recombinant protein (RP) in *Escherichia coli*, we constructed plasmid pGNMT-His-short. The large S-tag DNA fragment was excised from the pGNMT-His (9) using *Eco*RI and *Nde*I restriction enzymes

Fig. 1. Nuclear translocation of glycine *N*-methyltransferase (GNMT) after cell treatment with benzo(*a*)pyrene. *A* and *B*, a double indirect immunofluorescent antibody assay was performed on HA22T/VGH cells transfected with pGNMT. Antisera: *A*, rabbit anti-GNMT antibody; *B*, mouse anti-FLAG antiserum. *C–F*, indirect immunofluorescent antibody assay on Huh7 cells transfected with pGNMT and treated with either DMSO solvent (*C* and *D*) or benzo(*a*)pyrene (*E* and *F*) before being fixed and reacted with mouse anti-FLAG antiserum. Immunofluorescent staining was performed with rhodamine-conjugated goat antirabbit antibodies (*A*) or FITC-conjugated rabbit antimouse antibodies (*B–F*). Nuclei were stained with Hoechst H33258.
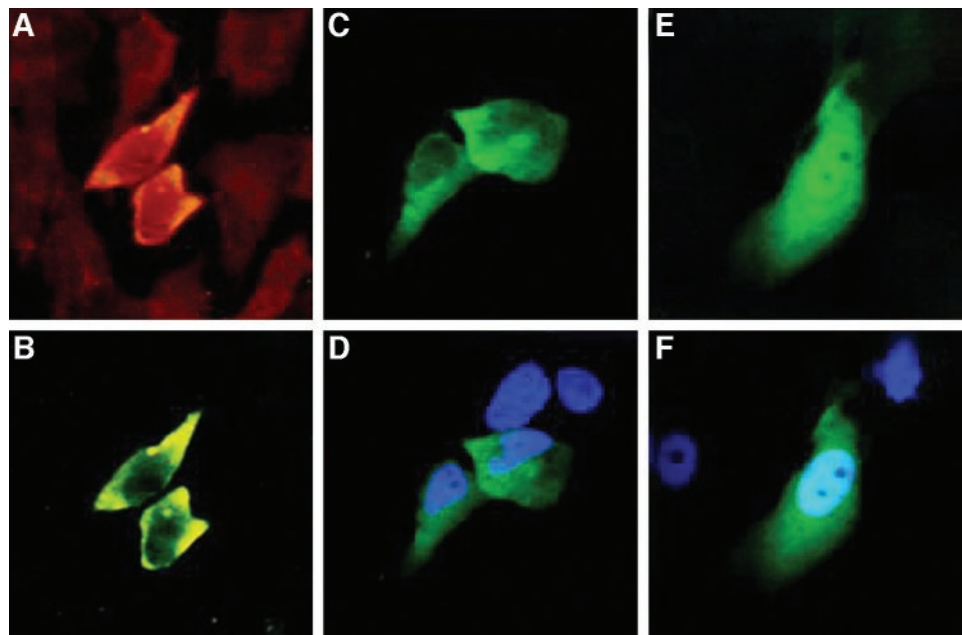
(Stratagene, La Jolla, CA); the resulting plasmid DNA was religated after a Klenow reaction. Plasmid DNA sequences were confirmed with a DNA sequencer equipped with a dye terminator cycle sequencing core kit (Applied Biosystems Model 373A, Version 1.0.2; Applied Biosystems, Foster City, CA).

GNMT RP Expression and Purification. pGNMT-His-short was used to transform the *E. coli* BL21 bacteria used for isopropyl-1-thio-β-D-galactopyranoside induction (induction time, 3 h; bacterial culture absorbance, 0.6–0.7). GNMT RP purification was performed using a Ni^{2+}-charged histidine-binding resin column according to the manufacturer's guidelines (Novagen, Madison, WI). RP concentration was measured with a BCA protein assay (Pierce, Rockford, IL); purity was tested by running samples on a 12.5% SDS-polyacrylamide mini-gel (Bio-Rad Laboratories, Richmond, CA).

Transfection. All plasmid DNA samples were prepared using Qiagen mega kits (Hilden, Germany). Standard calcium phosphate coprecipitation methodology (16) was used to transfect cultured cells from various liver cancer cell lines with plasmid DNA. Forty-eight h after transfection, cells were treated with different concentrations (1–10 μM) of BaP (Sigma-Aldrich, Steinheim, Germany) dissolved in DMSO (Nacalaitesque, Osaka, Japan) for 16 h. Treated cells were subjected to either indirect immunofluorescent antibody assay or ^{32}P postlabeling. To produce a negative control, 0.1% DMSO was added to the cell culture.

Establishing Stable Clones Expressing GNMT. Using calcium phosphate methodology, HepG2 cells were cotransfected with pGNMT and pTK-Hyg (Clontech, Palo Alto, CA) plasmid DNAs. Cells were placed in a selection medium containing 300 μg/ml hygromycin (17). More than 12 clones were selected, and GNMT expression was analyzed with a Western blot (WB) assay using cell lysate collected from each clone. Among them, SCG2--1-1 and SCG2-1-11 were chosen for further study based on their expression level of GNMT. SCG2-neg, a stable clone selected from HepG2 cells cotransfected with pFLAG-CMV-5 and pTK-Hyg plasmids, was also used as a control in this study.

Indirect Immunofluorescent Antibody Assay. Cultured HA22T/VGH or Huh7 cells were placed on cover slides, treated with 10 μM BaP or 0.1% DMSO, fixed with solution I (4% paraformaldehyde and 400 mM sucrose in PBS) at 37°C for 30 min, fixed with solution II (fixing solution I plus 0.5% Triton X-100) at room temperature for 15 min, and fixed with blocking buffer (0.5% BSA in PBS) at room temperature for 1 h. After washing with PBS, the slides were allowed to react with various primary antibodies at 4°C overnight. The two antibodies were anti-FLAG monoclonal antibody (1:500 dilution; Kodak) and rabbit anti-GNMT antiserum-R4 (1:200 dilution; Ref. 12). FITC-conjugated antimouse IgG and tetramethylrhodamine isothiocyanate-conjugated antirabbit IgG (Sigma-Aldrich) were used as secondary antibodies. After

four washes with PBS, slides were mounted and observed using a confocal fluorescence microscope (TCS-NT, Hilden, Germany). DNA was stained with Hoechst H33258 (Sigma-Aldrich) to localize cell nuclei.

Generating Adenovirus Carrying GNMT cDNA (Ad-GNMT). To construct a GMNT recombinant adenovirus controlled by a CMV promoter, pGEX-GNMT (9) was digested with *Xho*I (filled-in) and *Bam*HI before insertion into the *Xba*I (filled-in) and *Bam*HI sites of pBluescript SK(−) (Stratagene). GNMT cDNA was also cloned into the *Hin*dIII and *Not*I sites of pAdE1CMV/pA (18), a shuttle vector containing the left arm of a virus genome, to generate pXCMV-GNMT. A recombinant adenovirus appeared within 7–12 days after the cotransfection of pXCMV-GNMT and pJM17 (18) into 293 cells. Individual virus clones were isolated and identified using PCR with primer sets specific to the adenoviral sequence (18), the insertion flanking regions (18), and the GNMT cDNA (8). Virus titer was determined via the plaque assay method described above (18).

^{32}P Postlabeling and Five-Dimensional TLC for Quantifying BPDE-DNA Adducts. We used SCG2 cells and hepatocellular carcinoma cell lines transiently transfected with pGNMT plasmid DNA for 48 h for our experiments. DNA was extracted from cells treated with 10 μM BaP or 0.1% DMSO (control) for 16 h (19) and digested with micrococcal endonuclease and spleen phosphodiesterase in succinate buffer (20 mM sodium succinate and 10 mM $CaCl_2$) for 3 h at 37°C. The resulting 3′ nucleotides were further extracted twice with butanol solution and labeled with [γ-^{32}P]ATP with T4 kinase in labeling buffer at 38°C for 30 min. Five-dimensional TLC was used to elucidate labeled DNA adducts (20). Relative adduct level was calculated as cpm in adducted nucleotides/(cpm in total nucleotides $\times$ dilution).

Aryl Hydrocarbon Hydroxylase Assay. To measure CYP1A1 enzyme activity, approximately 100 μg of cellular homogenates were incubated with reactive solution (100 mM HEPES, 0.4 mM NADPH, 1 mM $MgCl_2$, and 20 μM BaP) at 37°C for 10 min. Supernatant protein concentrations were determined

Table 1 *Effects of GNMT[a] expression on BPDE-DNA adduct formation in HCC cell lines*

Cells transfected with[c]	BPDE-DNA adducts (RAL) in[b]		
	HepG2	Huh7	HA22T/VGH
pGNMT	261.4 (47.2%)	70.9 (86.5%)	86.6 (79.3%)
pCMV vector	553.5 (100%)	82.0 (100%)	109.1 (100%)
No transfection	625.0	NT	161.7

[a] GNMT, glycine *N*-methyltransferase; BPDE, benzo(*a*)pyrene-7,8-diol 9,10-epoxide; HCC, hepatocellular carcinoma; RAL, relative adduct level; NT, not tested.
[b] RAL/10^8 nucleotides; measured by ^{32}P postlabelingmethod.
[c] Transfection efficiency: HepG2, 30%; Huh7,45%; HA22T/VGH, 60%.
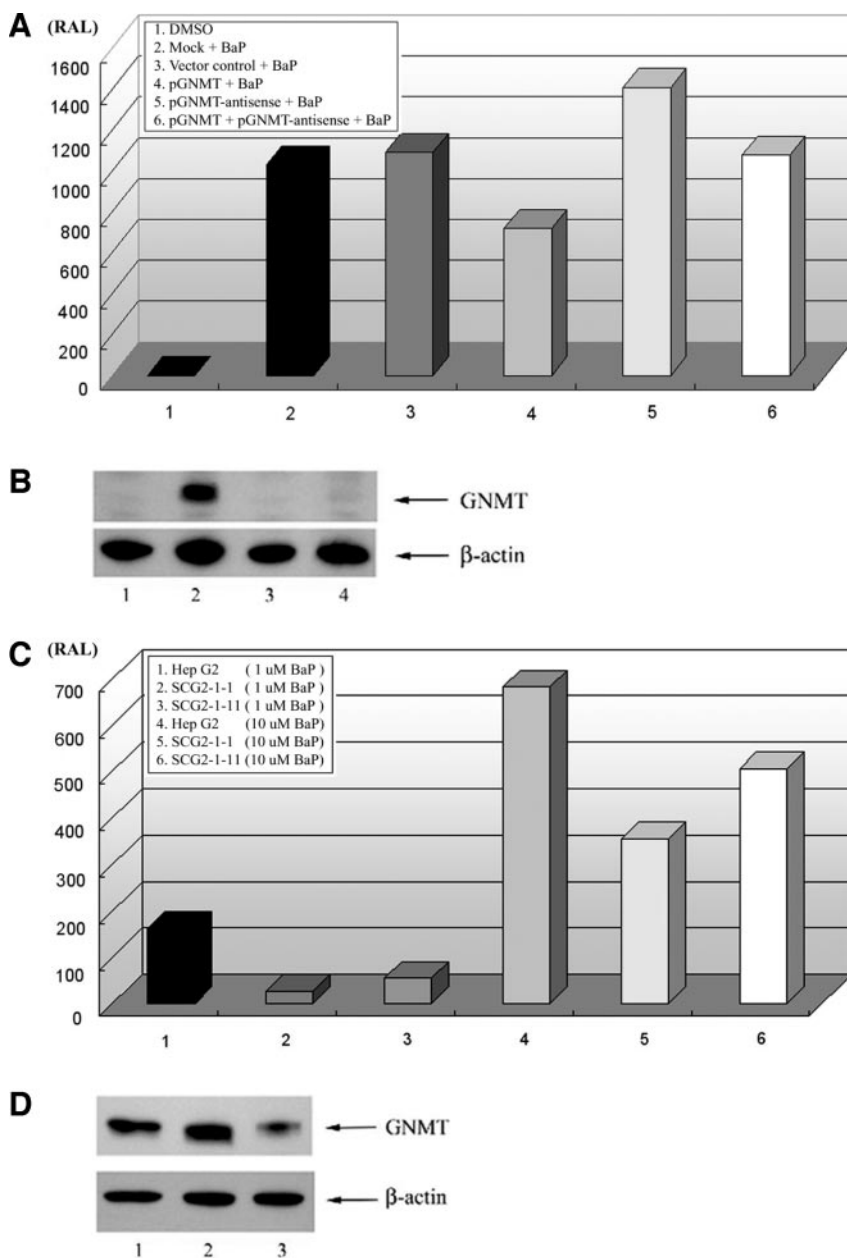
Fig. 2. Effects of glycine *N*-methyltransferase (GNMT) on benzo(*a*)pyrene-7,8-diol 9,10-epoxide (BPDE)-DNA adduct formation. *A,* amount (relative adduct level) of BPDE-DNA adducts using a combination of ^{32}P postlabeling and five-dimensional TLC. *1,* DMSO solvent control; *2,* mock transfection; *3,* cells transfected with 40 μg of control (pFLAG-CMV-5) vector; *4,* cells transfected with 40 μg of pGNMT; *5,* cells transfected with 40 μg of pGNMT-antisense; *6,* cells cotransfected with 20 μg of pGNMT and 20 μg of pGNMT-antisense. DNA adduct quantities/10^8 nucleotides (relative adduct level) were as follows: *1,* 0; *2,* 1031.7; *3,* 1092.4; *4,* 719.8; *5,* 1411.3; *6,* 1079.7. *B,* Western blot analysis of GNMT expression in HepG2 cells transfected with the control (pFLAG-CMV-5) vector (*Lane 1*), pGNMT (*Lane 2*), pGNMT-antisense (*Lane 3*), or pGNMT/pGNMT-antisense (*Lane 4*). *Bottom row* shows β-actin expression levels for the four experiments. *C,* amounts of of BPDE-DNA adducts in HepG2, SCG2-1-1, and SCG2-1-11 cells treated with 1 or 10 μM benzo(*a*)pyrene (BaP). *1* and *4,* HepG2 cells treated with 1 or 10 μM BaP; *2* and *5,* SCG2-1-1 cells treated with 1 or 10 μM BaP; *3* and *6,* SCG2-1-11 cells treated with 1 or 10 μM BaP. DNA adduct quantities/10^8 nucleotides (relative adduct level) were as follows: *1,* 161.9; *2,* 26.4; *3,* 55.2; *4,* 682.1; *5,* 354.9; *6,* 506.5. *D,* Western blot analysis of GNMT expression in HepG2 (*Lane 1*), SCG2-1-1 (*Lane 2*), and SCG2-1-11 (*Lane 3*) cells. Twenty μg of cell lysates from each cell line were used for the PAGE. *Bottom row* shows β-actin expression levels for the four experiments.

using a Bio-Rad protein assay kit (Hercules, CA). Reactions were stopped by the addition of acetone; extraction was performed with hexane and 1N NaOH. NaOH fractions were read on a spectrofluorometer (Hitahi Instrument F4500) with excitation and emission wavelengths of 396 nm and 522 nm, respectively. Reaction product (3-hydroxy-BaP) concentrations were calculated by comparison with a standard; procedural details are given in Ref. 21.

WB Assay. WB was used to detect GNMT in transfected cells or SCG2 clones. Anti-GNMT monoclonal antibody 14-1 was used to detect GNMT (9). A detailed description of WB procedures is presented in Ref. 22.

LGA Dockings. LGA was used to elucidate interaction sites between BaP and various forms of GNMT. Autodock 3.0 software was used to identify the most favorable ligand binding interactions. We empirically determined van der Waals hydrogen bonding, hydrophobic desolvations, and electrostatic and torsional free energy to reproduce ligand-protein binding free energies (23). We used X-ray crystallography data from rat GNMT for docking due to its 91% amino acid sequence homology with human GNMT (24, 25). We analyzed interactions between BaP and methyltransferase-1VID (26), 1HMY (27), 2ADM (28), 1DCT (29), 1BOO (30), 2DPM (31), 1EG2 (32), and 1G55 (33). Parameters were as follows: 10 runs; a population size of 50; and a run-termination criterion of a maximum of 27,000 generations or 2.5×10^5 energy

evaluations, whichever came first. A root mean square deviation conformational clustering tolerance of 0.5 Å was calculated from the ligand's crystallographic coordinates. Procedural details are available in Ref. 34.

GNMT Enzyme Activity Assay. GNMT RP purified from a Ni^{2+}-charged histidine-binding resin column was used for an enzyme activity assay. GNMT RP (10 mg) was mixed with 10, 50, or 100 μM BaP or DMSO solvent (control) at room temperature for 60 min before treatment with 100 μl of 100 mM Tris buffer (pH 7.4) containing 50 mM glycine, 0.23 mM SAM, and 2.16 μM *S*-adenosyl-L-[*methyl*-^{3}H]methionine (76.4 Ci/mmol). After incubation at 37°C for 30 min, individual reactions were terminated by the addition of a 50-μl mixture of 10% trichloroacetic acid and 5% activated charcoal. Each reaction was performed in triplicate. This procedure has been described in detail by Cook and Wagner (35).

RESULTS

GNMT Nuclear Translocation Was Induced by BaP in Both HA22T/VGH and Huh7 Cells. GNMT was expressed in the cytoplasm of HA22T/VGH cells 48 h after transfection with pGNMT
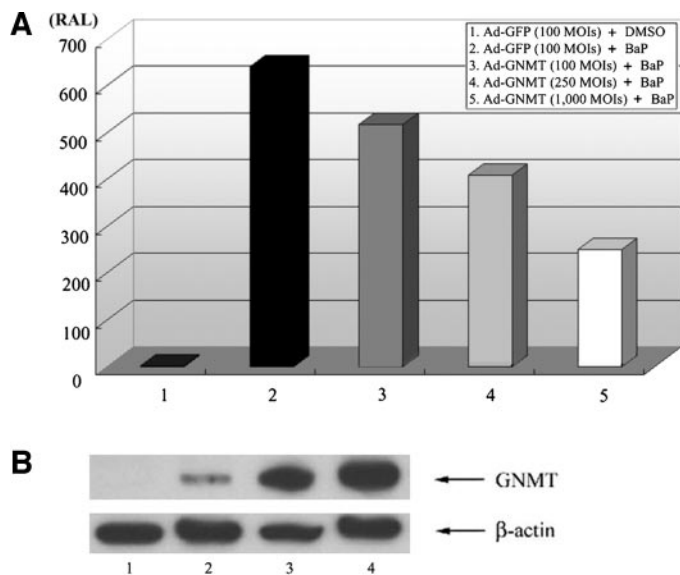
Fig. 3. Effects of glycine *N*-methyltransferase (GNMT) expression on benzo(*a*)pyrene (BaP)-7,8-diol 9,10-epoxide-DNA adduct formation in HepG2 cells infected with Ad-GFP or various MOIs of Ad-GNMT. *A*: *1*, cells infected with Ad-GFP and treated with DMSO solvent; *2*, cells infected with Ad-GFP and treated with BaP; *3*, cells infected with MOI = 100 of Ad-GNMT and treated with BaP; *4*, cells infected with MOI = 250 of Ad-GNMT and treated with BaP; *5*, cells infected with MOI = 1000 of Ad-GNMT and treated with BaP. DNA adduct quantities/10^8 nucleotides (relative adduct level) were as follows: *1*, 0; *2*, 638.9; *3*, 514.2; *4*, 405.3; *5*, 224.3. *B*, Western blot analysis of GNMT expression in the same experiment. *Lane 1*, Ad-GFP control; *Lane 2*, Ad-GNMT (MOI = 100); *Lane 3*, Ad-GNMT (MOI = 250); *Lane 4*, Ad-GNMT (MOI = 1000).

DNA (double indirect immunofluorescent antibody assay with both rabbit anti-GNMT antiserum and mouse anti-FLAG monoclonal antibody; Fig. 1, *A* and *B*). Similar results were noted in control Huh7 cells treated with DMSO solvent (Fig. 1, *C* and *D*). In contrast, GNMT proteins were only partly translocated into the nuclei of Huh7 cells treated with 10 μM BaP for 16 h (Fig. 1, *E* and *F*). DNA was stained with Hoechst H33258 to localize cell nuclei (Fig. 1, *D* and *F*).

Inhibitory Effect of GNMT on BPDE-DNA Adduct Formation.
^{32}P postlabeling and five-dimensional TLC were used to quantify BPDE-DNA adduct formation. After treatment with 10 μM BaP for 16 h, BPDE-DNA adduct formation in HepG2, Huh7, and HA22T/VGH cells transfected with pGNMT decreased 52.8%, 13.5%, and 20.7%, respectively, compared with cells transfected with the vector plasmid (Table 1). Because the inhibitory effect of GNMT on BPDE-DNA adduct formation was strongest in the HepG2 cells, we used that cell line as the target in subsequent experiments. HepG2 cell DNA transfection efficiency was approximately 30%. In addition to pGNMT, a plasmid containing an antisense GNMT sequence was constructed for the purpose of verifying the specificity of the GNMT effect. After BaP treatment, a 34.1% decrease was noted in BPDE adducts formed in pGNMT-transfected cells compared with cells transfected with the vector control plasmid (Fig. 2*A, 3* and *4*). In contrast, a 29.2% increase in BPDE adducts was noted in HepG2 cells transfected with pGNMT-antisense (Fig. 2*A, 5*). Quantities of BPDE-DNA adducts formed in cells transfected with equal amounts (20 μg) of pGNMT and pGNMT-antisense were approximately equal to those formed in the vector control cells (Fig. 2*A, 6*). GNMT expression in different transfection experiments and the effects of antisense GNMT cDNA plasmid construct (pGNMT-antisense) were verified by WB assays with mouse anti-GNMT monoclonal antibody. As shown in *Lane 4* of Fig. 2*B*, GNMT was not detected in the lysates of cells transfected with equal amounts of pGNMT and pGNMT-antisense.

We used two stable clones (SCG2-1-1 and SCG2-1-11) from HepG2 cells transfected with pGNMT in the same experiments de-

scribed above. Results from a Northern blot assay indicate that copy numbers (per cell) of GNMT cDNA present in SCG2-1-1 and SCG2-1-11 cells were 3 and 1, respectively (data not shown). Results from a WB assay showed that the GNMT expression level in the SCG2-1-1 cells was nearly three times that in the SCG2-1-11 cells (Fig. 2*D*, *Lanes 2* and *3*). After treating the SCG2-1-1 and SCG2-1-11 cells with 1 or 10 μM BaP, BPDE-DNA adduct formation inhibition was proportional to GNMT-expression levels under both treatment conditions (Fig. 2*C*).

We performed the same experiment using an adenovirus carrying GNMT cDNA (Ad-GNMT). A positive linear relationship was noted between the multiplicities of infection (MOIs) of the Ad-GNMT and BPDE-DNA-adduct formation inhibition (Fig. 3). Compared with Ad-GFP-control-infected cells, the Ad-GNMT MOIs increased from 100 to 250 to 1000, and BPDE-DNA adduct formation decreased 19.5%, 36.6%, and 61.8%, respectively (Fig. 3*A*). GNMT expression levels in HepG2 cells infected with MOI = 100 of Ad-GFP control and MOI = 100, 250, and 1000 of Ad-GNMT were analyzed by WB; results are shown in Fig. 3*B, Lanes 1–4*.

GNMT Effect on CYP1A1 Enzyme Activity Induced by BaP.
SCG2-1-1 and SCG2-neg cells were treated with varying concentrations of BaP for 16 h before using aryl hydrocarbon hydroxylase assay to measure their cellular CYP1A1 enzyme activity. CYP1A1 activity in cells treated with 3, 6, and 9 μM BaP was 24.5, 41.5 and 71.3 pmol/mg/min for SCG2-neg cells, respectively, and 20.1, 27.7, and 36.2 pmol/mg/min for SCG2-1-1 cells, respectively (Fig. 4). For cells treated with 9 μM BaP, this represents a 45% reduction in CYP1A1 enzyme activity in GNMT-expressing cells (*i.e.*, SCG2-1-1) compared with SCG2-neg cells.

Modeling GNMT-BaP Interaction. We used a LGA to predict physical GNMT-BaP interaction. Again, due to its 91% homology with human GNMT proteins, rat GNMT X-ray crystallography was used for the BaP docking experiments. As shown in Fig. 5, *A* and *B*, we found that BaP binds with both dimeric (*yellow*) and tetrameric (*cyan*) forms of GNMT but that it prefers binding with the dimeric form (Protein Data Bank code 1D2C). This cluster is located at the intersection of the SAM- and *S*-adenosylhomocystine-binding sites (Table 2; Fig. 5*B*). The low (-9.10 kcal/mol) binding energy between the dimeric form of GNMT and BaP suggests that BaP may displace
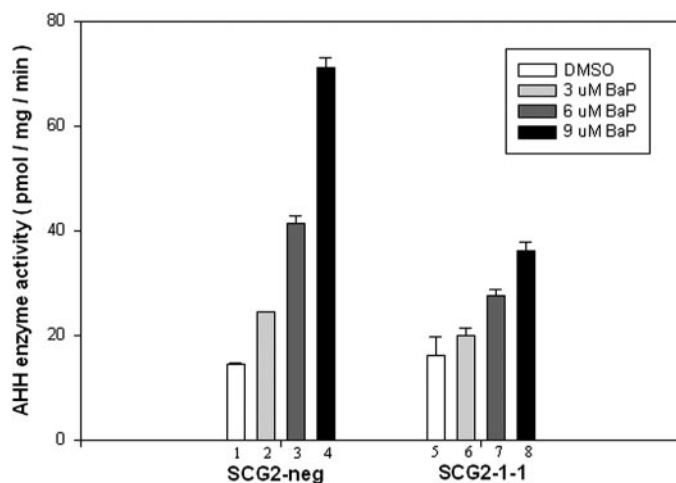
Fig. 4. Cytochrome P450 1A1 (CYP1A1) enzyme activity induced by benzo(*a*)pyrene (BaP) in SCG2-neg and SCG2-1-1 cells as measured by an aryl hydrocarbon hydroxylase (AHH) assay. *1–4*, CYP1A1 activity in SCG2-neg cells; *5–8*, CYP1A1 activity in SCG2-1-1 cells. Treatments were as follows: *1* and *5*, DMSO solvent; *2* and *6*, 3 μM BaP; *3* and *7*, 6 μM BaP; *4* and *8*, 9 μM BaP. The CYP1A1 enzyme activity [means (in pmol/mg/min) and SDs (in parentheses)] was as follows: *1*, 14.5 (0.27); *2*, 24.47 (0.14); *3*, 41.5 (1.42); *4*, 71.3 (1.75); *5*, 16.2 (3.6); *6*, 20.1 (1.5); *7*, 27.7 (1.2); *8*, 36.2 (1.7).
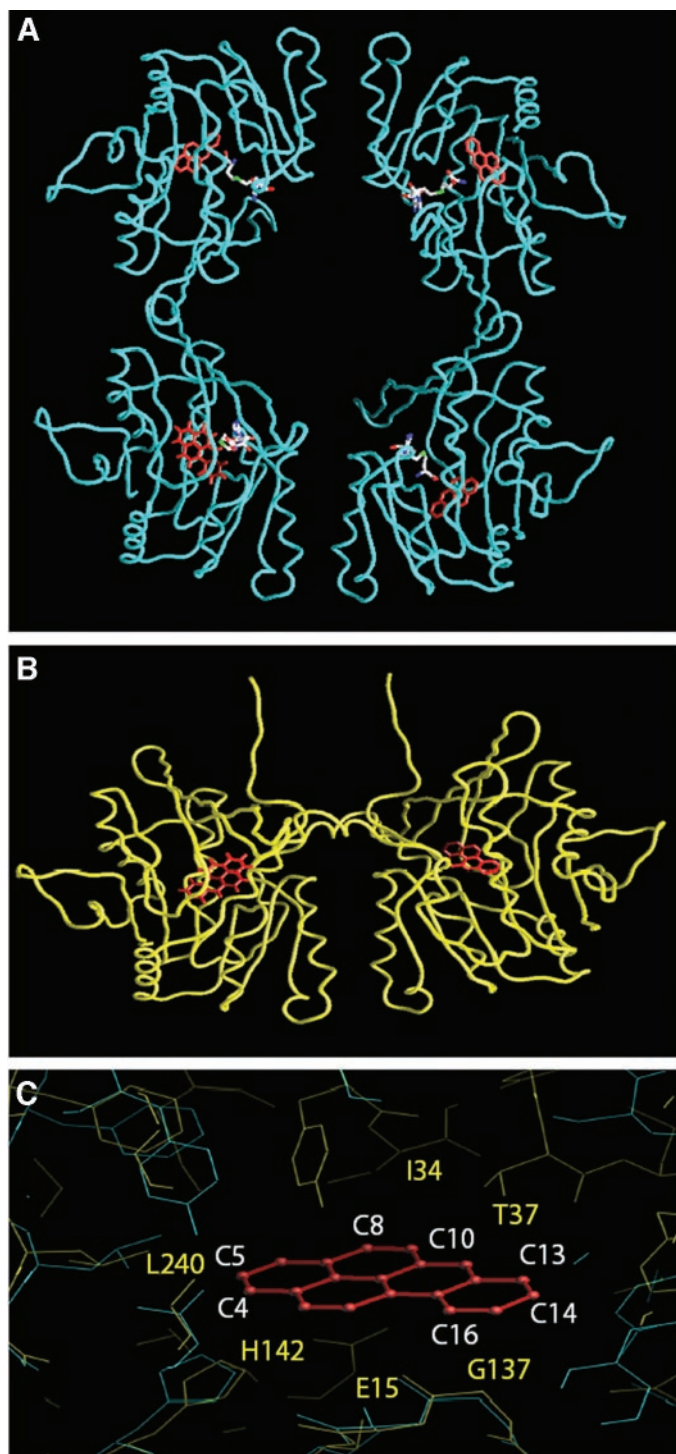
Fig. 5. Model of benzo(*a*)pyrene (BaP) docking with dimeric and tetrameric forms of GNMT using the Lamarckian genetic algorithm. *A,* BaP (*red*) docked with *S*-adenosyl-homocystine (*white*)-bound tetrameric form of rat glycine *N*-methyltransferase [GNMT (*cyan*; Protein Data Bank code 1D2H)]. *B,* BaP (*red*) docked with the dimeric form of rat GNMT (*yellow*; Protein Data Bank code 1D2C). *C,* dimeric form of GNMT (*yellow*) superimposed on tetrameric form of GNMT (*cyan*). GNMT amino acid residues (Ile[34], Thr[37], Gly[137], His[142], and Leu[240] of one dimeric subunit and Glu[15] of another) in close proximity to several BaP carbon atoms are indicated based on Protein Data Bank code 1D2C and BaP docking model.

the SAM position; the high (254.9 kcal/mol) binding energy of BaP with a GNMT dimer already bound with SAM (Protein Data Bank code 1XVA) suggests that BaP and SAM are in competition for binding with GNMT (Table 2). Accordingly, several GNMT amino

acid residues (including Thr[37], Gly[137], and His[142] of one dimer subunit and Glu[15] of another subunit) are in close proximity to BaP (Fig. 5*C*).

BaP-Induced Inhibition of GNMT Enzyme Activity. Based on the inference that BaP can bind with GNMT, we studied the potential effects of BaP on GNMT enzyme activity by constructing plasmid pGNMT-His-Short to express a His-tag-GNMT RP in *E. coli*. GNMT RP purified from a Ni^{2+}-charged histidine-binding resin column was used for our analysis. As shown in Fig. 6, GNMT enzyme activity from reactions containing 10 and 50 μM BaP decreased 44% and 62%, respectively, compared with the DMSO control.

DISCUSSION

We used an indirect immunofluorescent antibody assay to demonstrate the power of BaP to induce the nuclear translocation of GNMT. Our results show that GNMT not only inhibits BPDE-DNA adduct formation but also down-regulates CYP1A1 enzyme activity; conversely, BaP also inhibits GNMT enzyme activity. Finally, we used a docking experiment to show the exact location of BaP-GNMT interaction. These results represent a novel finding of a cellular defense mechanism against potentially damaging forms of exposure. We confirmed the inhibition of BPDE-DNA adduct formation by GNMT via transient transfection, stable clone selection, and adenovirus infection systems, with consistent results throughout. An antisense construct for GNMT cDNA was used to demonstrate interaction specificity (Fig. 2*A*), and WB assays were used to monitor GNMT expression levels in various gene transfer experiment sets. The dose-dependent inhibitory effect of GNMT on BPDE-DNA adduct formation was further elaborated with HepG2 stable clones and a recombinant adenovirus carrying GNMT cDNA (Figs. 2*C* and 3*A*).

Many polycyclic aromatic hydrocarbons induce cytochrome P450 expression through an AhR-dependent pathway (36). After diffusing into a cell, BaP binds with AhR and translocates into the nuclei, where BaP-AhR heterodimers form complexes with Ah receptor nuclear translocator (Arnt) proteins (2). The BaP-AhR-Arnt complexes then transactivate the CYP1A1 gene via interaction with its xenobiotic responsive element in the promoter region (37). In addition to the inhibition of BPDE-DNA adduct formation, our results show that GNMT is capable of reducing CYP1A1 enzyme activity induced by BaP (Fig. 4). Foussat *et al.* (38) used AhR-deficient transgenic mice to demonstrate that GNMT is not a transcriptional activator of the CYP1A1 gene (38). Preliminary data from our real-time PCR analysis showed that after BaP treatment, CYP1A1 gene expression was reduced by approximately 20% in SCG2-1-1 cells compared with HepG2 cells.[5]

Previous research has shown that the tetrameric form of rat GNMT acts as an enzyme and that the dimeric form of rat GNMT is capable of binding with polycyclic aromatic hydrocarbons (39). In this study, we used LGA and a scoring function for estimating binding-related free energy change to locate possible sites for interactions between BaP and various forms of GNMT; we used X-ray crystallography data for rat GNMT for this purpose. Our results indicate that (*a*) the BaP-binding domain is located at the substrate (SAM)-binding site of GNMT and (*b*) BaP prefers binding with the dimeric form of GNMT. The R175K mutant form of the GNMT tetramer (Protein Data Bank code 1D2G) was used to demonstrate that although the R/K residue is near the binding site ($\sim$5 Å from the SAM position), it exerts practically no effect on GNMT-BaP cluster formation (Table 2). In comparison, the presence of an acetate ion favors the formation of the

second preferred cluster in GNMT-SAM binding in the 1XVA crystal structure (Table 2, final entry). It has been demonstrated that of various search systems, the LGA method is the most likely to locate crystallographic structures (23). Heavily populated clusters usually correspond to crystallographically determined positions that show 0.2–0.8 Å root mean square differences from the crystal structures. For most ligands, our docking simulation predicted single binding modes that matched crystallographic binding modes within 1.0 Å root mean square deviation (23). We therefore suggest that the LGA is a reliable method for predicting the bound conformation of a ligand to its macromolecular target. BaP-GNMT interaction was also confirmed by a functional assay showing that GNMT enzyme activity was reduced nearly 50% in the presence of BaP (Fig. 6).

Because BaP prefers binding with the SAM-binding domain of GNMT, we used the LGA to study interactions between BaP and eight other SAM-dependent methyltransferases: catechol *O*-methyltransferase; *Hha*I DNA methyltransferase; *Taq*I DNA methyltransferase; *Hae*III DNA methyltransferase; *Pvu*II DNA methyltransferase; *Dpn*II DNA methyltransferase; *Rsr*I DNA methyltransferase; and DNA methyltransferase 2. Our results show that BaP was capable of binding with the *Hha*I, *Hae*III, and *Pvu*II DNA methyltransferases and DNA methyltransferase 2, but not with catechol *O*-methyltransferase or *Taq*I, *Dpn*II, and *Rsr*I DNA methyltransferases (Table 3). It is interesting to note that the target atom of all of the BaP-preferred DNA

Table 2 *Lamarckian genetic algorithm dockings of GNMT^a protein and BaP molecules*

PDB code[b]	Small molecule	Cluster no.	Cluster population	Mean energy (kcal/mol)	No. of evaluations	Protein details
1D2C[c]	BaP	1	10	−7.38	2.5×10^5	Apo GNMT dimer
1D2G[c]	BaP	1	10	−7.53	2.5×10^5	R175K mutant dimer
1D2H[c]	BaP	3	5	−3.22	2.5×10^5	R175K + SAH tetramer
1XVA[d]	BaP	5	5	+254.9	2.5×10^5	+SAM dimer
1XVA[e]	BaP	2	8	−9.10	2.5×10^5	−SAM dimer
1XVA[f]	SAM	2	5	−9.85	2.5×10^5	−SAM dimer

^a GNMT, glycine *N*-methyltransferase; BaP, benzo(*a*)pyrene; PDB, Protein Data Bank; SAH, *S*-adenosylhomocystine; SAM, *S*-adenosylmethionine; RMSD, root mean square deviation.
^b PDB (http://www.rcsb.org/pdb).
^c Cluster is located at the intersection of SAM and SAH.
^d BaP is ~2 Å from SAM; the high energy level suggests that such a complex is difficult to form.
^e BaP displaces the SAM position.
^f RMSD = 2.70 Å. A second cluster (n = 5) corresponds to the known crystal structure at an RMSD of 0.68 Å and a mean energy of −8.80 kcal/mol. Note the nearby location of an acetate ion that might serve to stabilize the second cluster.
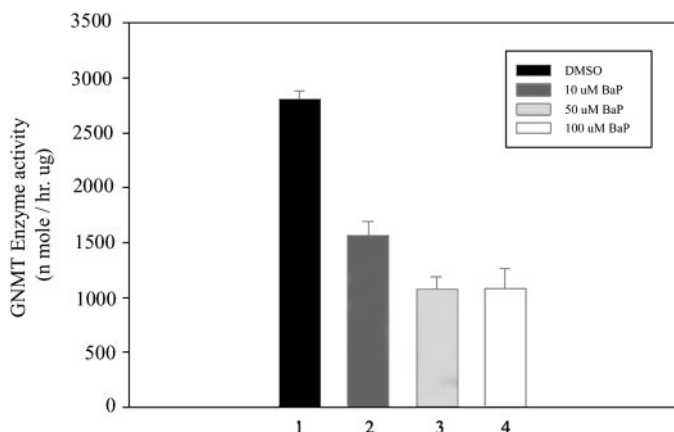
Fig. 6. Inhibition of glycine *N*-methyltransferase enzyme activity by benzo(*a*)pyrene (BaP). Glycine *N*-methyltransferase enzyme activity was measured as 2810.8 ± 73.7 nmol/h/μg for treatment with DMSO solvent, 1563.3 ± 127.4 nmol/h/μg for treatment with 10 μM BaP, 1069.5 ± 124.2 nmol/h/μg for treatment with 50 μM BaP, and 1083.3 ± 175.9 nmol/h/μg for treatment with 100 μM BaP. Each reaction set was performed in triplicate, as were individual experiments.

Table 3 *Lamarckian genetic algorithm dockings of some SAM^a-dependent methyltransferases and BaP molecules^b*

PDB code[c]	Small molecule	No. of clusters	Cluster population	Mean energy kcal/mol	No. of evaluations	Protein details
1VID[d]	BaP	2	4	−2.18	2.5×10^5	COMT monomer
1HMY[e]	BaP	3	8	−8.94	2.5×10^5	*Hha*I DNA MT monomer
2ADM[f]	BaP	4	6	+47.19	2.5×10^5	*Taq*I DNA MT dimer
1DCT[g]	BaP	3	8	−9.69	2.5×10^5	*Hae*III DNA MT dimer
1BOO[h]	BaP	3	5	−8.69	2.5×10^5	*Pvu*II monomer
2DPM[i]	BaP	4	5	+13.46	2.5×10^5	*Dpn*II DNA MT monomer
1EG2[j]	BaP	4	2	+85.64	2.5×10^5	*Rsr*I DNA MT monomer
1G55[k]	BaP	1	10	−8.70	2.5×10^5	DNMT2 DNA MT monomer

^a SAM, *S*-adenosylmethionine; BaP, benzo(*a*)pyrene; PDB, Protein Data Bank; COMT, catechol *O*-methyltransferase; MT, methyltransferase; DNMT2, DNA methyltransferase 2.
^b The SAM molecules were removed from the 1VID, 1HMY, 2ADM, and 2DPM methyltransferase macromolecules before docking. The BaP molecule tried to move into the former SAM position. The *S*-adenosylhomocystine molecules were removed from the 1BOO and 1G55 methyltransferase macromolecules before docking.
^c PDB (http://www.rcsb.org/pdb).
^d The energy of the second cluster (population 6/10) was −0.32 kcal/mol; COMT did not bind with BaP at one preferred position.
^e The energy of the second cluster (population 1/10) was −6.45 kcal/mol; *Hha*I DNA MT bound with BaP at a lower energy-preferred position.
^f The high binding energy (+47.19 kcal/mol) suggests that *Taq*I DNA MT does not bind with BaP.
^g The energy of the second cluster (population 1/10) was −9.50 kcal/mol, very close to the lowest energy cluster (population 8/10, energy −9.69 kcal/mol); therefore, *Hae*III DNA MT bound strongly with BaP at a preferred position.
^h The high binding energy (−8.69 kcal/mol) suggests that *Pvu*II binds with BaP. The binding energies of the other two observed clusters (−8.63 kcal/mol and −8.58 kcal/mol) were very close to the lowest energy cluster.
^i The +13.46 kcal/mol binding energy suggests that *Dpn*II DNA MT does not bind with BaP.
^j The +85.64 kcal/mol binding energy suggests that *Rsr*I DNA MT does not bind with BaP.
^k The −8.70 kcal/mol binding energy suggests that DNMT2 binds strongly with BaP in a preferred position.

methyltransferases is cytosine and not adenine (40). To our knowledge, this is the first evidence suggesting that an environmental carcinogen such as BaP has the potential to interact with different DNA methyltransferases. In light of evidence showing that the induction of GNMT enzyme activity by all-*trans*-retinoic acid causes DNA hypomethylation in rat hepatocytes (22), we suggest that BaP may affect DNA methylation via interactions with DNA methyltransferase and GNMT and thus contribute to a carcinogenic pathway.

ACKNOWLEDGMENTS

REFERENCES

1. Fischman ML, Cadman EC, Desmond S. Occupational cancer. In: LaDou J, editor. Occupational medicine. Norwalk, CT: Appleton and Lange; 1990. p. 182–208.
2. Whitlock JP Jr, Okino ST, Dong L, et al. Cytochromes P450 5: induction of cytochrome P4501A1: a model for analyzing mammalian gene transcription. FASEB J 1996;10:809–18.
3. Foldes RL, Hines RN, Ho KL, et al. 3-Methylchlanthrene-induced expression of the cytochrome P-450c gene. Arch Biochem Biophys 1985;239:137–46.
4. Raval P, Iversen PL, Bresnick E. Induction of cytochromes P450IA1 and P450IA2 as determined by solution hybridization. Biochem Pharmacol 1991;41:1719–23.

5. Wijnhoven SW, Kool HJ, van Oostrom CT, et al. The relationship between benzo-[a]pyrene-induced mutagenesis and carcinogenesis in repair-deficient Cockayne syndrome group B mice. Cancer Res 2000;60:5681–7.

6. Kerr SJ. Competing methyltransferase system. J Biol Chem 1972;247:4248–52.

7. Yeo EJ, Wagner C. Tissue distribution of glycine N-methyltransferase, a major folate-binding protein of liver. Proc Natl Acad Sci USA 1994;91:210–4.

8. Chen YMA, Shiu JY, Tzeng SJ, et al. Characterization of glycine-N-methyltransferase-gene expression in human hepatocellular carcinoma. Int J Cancer 1998;75:787–93.

9. Liu HH, Chen KH, Lui WY, Wong FW, Chen YMA. Characterization of reduced expression of glycine N-methyltransferase in the cancerous hepatic tissues using two newly developed monoclonal antibodies. J Biomed Sci 2003;10:87–97.

10. Chen YMA, Chen LY, Wong FH, et al. Genomic structure, expression and chromosomal localization of the human glycine N-methyltransferase gene. Genomics 2000;66:43–7.

11. Tseng TL, Shih YP, Huang YC, et al. Genotypic and phenotypic characterization of a putative tumor susceptibility gene, GNMT, in liver cancer. Cancer Res 2003;63:647–54.

12. Raha A, Wagner C, MacDonald RG, Bresnick E. Rat liver cytosolic 4 S polycyclic aromatic hydrocarbon-binding protein is glycine N-methyltransferase. J Biol Chem 1994;269:5750–6.

13. Nakabayashi H, Taketa K, Miyano K, Yamane T, Sato J. Growth of human hepatoma cell lines with differentiated functions in chemically defined medium. Cancer Res 1982;42:3858–63.

14. Fogh J, Trempe G, Loveless JD. New human tumor cell lines. In: Fogh J, editor. Human tumor cells in vitro. New York: Plenum Press; 1977. p. 115–9.

15. Aden DP, Fogel H, Plotkin S, Damjanov I, Knowles BB. Controlled synthesis of HbsAg in a differentiated human liver-carcinoma-derived cell line. Nature (Lond) 1979;282:615–6.

16. Clark SJ, Harrison J, Paul CL, Frommer M. High sensitivity mapping of methylated cytosines. Nucleic Acids Res 1994;22:2990–7.

17. Gurtu V, Yan G, Zhang G. IRES bicistronic expression vectors for efficient creation of stable mammalian cell lines. Biochem Biophys Res Commun 1996;229:295–8.

18. Kleinerman D, Zhang WW, von Eschenbach AC, Lin S-H, Hsieh JT. Application of a tumor suppressor gene, C-CAM1, in androgen-independent prostate cancer therapy: a preclinical study. Cancer Res 1995;55:2831–6.

19. Vesselinovitch SD, Koka M, Mihailovich N, Rao KVN. Carcinogenicity of diethylnitrosamine in newborn, infant and adult mice. J Cancer Res Clin Oncol 1984;108:60–5.

20. Roggeband R, Wolterbeek AP, Rutten AA, Baan RA. Comparative ^{32}P-postlabeling analysis of benzo[a]pyrene-DNA adducts formed in vitro upon activation of benzo-[a]pyrene by human, rabbit and rodent liver microsomes. Carcinogenesis (Lond) 1993;14:1945–50.

21. Chang KW, Lee H, Wang HJ, Chen SY, Lin P. Differential response to benzo-[a]pyrene in human lung adenocarcinoma cell lines: the absence of aryl hydrocarbon receptor activation. Life Sci 1999;65:1339–49.

22. Rowling MJ, McMullen MH, Schalinske KL. Vitamin A and its derivatives induce hepatic glycine N-methyltransferase and hypomethylation of DNA in rats. J Nutr 2002;132:365–9.

23. Rosenfeld RJ, Goodsell DS, Musah RA, et al. Automated docking of ligands to an artificial active site: augmenting crystallographic analysis with computer modeling. J Comput Aid Mol Des 2003;17:525–36.

24. Fu Z, Hu Y, Konishi K, et al. Crystal structure of glycine N-methyltransferase from rat liver. Biochemistry 1996;35:11985–93.

25. Huang Y, Komoto J, Konishi K, et al. Mechanisms for auto-inhibition and forced product release in glycine N-methyltransferase: crystal structures of wild-type, mutant R175K and S-adenosylhomocysteine-bound R175K enzymes. J Mol Biol 2000;298:149–62.

26. Vidgren J, Svensson LA, Liljas A. Crystal structure of catechol O-methyltransferase. Nature (Lond) 1994;368:354–8.

27. Cheng X, Kumar S, Posfai J, Pflugrath JW, Roberts RJ. Crystal structure of the HhaI DNA methyltransferase complexed with S-adenosyl-L-methionine. Cell 1993;74:299–307.

28. Schluckebier G, Kozak M, Bleimling N, Weinhold E, Saenger W. Differential binding of S-adenosylmethionine, S-adenosylhomocysteine and Sinefungin to the adenine-specific DNA methyltransferase M.TaqI. J Mol Biol 1997;265:56–67.

29. Reinisch KM, Chen L, Verdine GL, Lipscomb WN. The crystal structure of HaeIII methyltransferase convalently complexed to DNA: an extrahelical cytosine and rearranged base pairing. Cell 1995;82:143–53.

30. Gong W, O'Gara M, Blumenthal RM, Cheng X. Structure of pvu II DNA-(cytosine N4) methyltransferase, an example of domain permutation and protein fold assignment. Nucleic Acids Res 1997;25:2702–15.

31. Tran PH, Korszun ZR, Cerritelli S, Springhorn SS, Lacks SA. Crystal structure of the Dpnm DNA adenine methyltransferase from the DpnII restriction system of Streptococcus pneumoniae bound to S-adenosylmethionine. Structure 1998;6:1563–75.

32. Scavetta RD, Thomas CB, Walsh M, et al. Structure of RsrI methyltransferase, a member of the N6-adenine B class of DNA methyltransferases. Nucleic Acids Res 2000;28:3950–61.

33. Dong A, Yoder JA, Zhang X, Zhou L, Bestor TH, Cheng X. Structure of human Dnmt2, an enigmatic DNA methyltransferase homolog that displays denaturant-resistant binding to DNA. Nucleic Acids Res 2001;29:439–48.

34. Morris GM, Goodsell DS, Halliday RS, et al. Automated docking using a Lamarckian genetic algorithm and an empirical binding free energy function. J Comput Chem 1998;19:1639–62.

35. Cook RJ, Wagner C. Glycine N-methyltransferase is a folate binding protein of rat liver cytosol. Proc Natl Acad Sci USA 1984;81:3631–4.

36. Okey AB, Bendy GP, Mason ME, et al. Temperature-dependent cytosol-to-nucleus translocation of the Ah receptor for 2,3,7,8-tetrachlorodibenzo-p-dioxin in continuous cell culture lines. J Biol Chem 1980;255:11415–22.

37. Hapgood J, Cuthill S, Denis M, Poellinger L, Gustafsson JA. Specific protein-DNA interactions at a xenobiotic-responsive element: copurification of dioxin receptor and DNA-binding activity. Proc Natl Acad Sci USA 1989;86:60–4.

38. Foussat J, Costet P, Galtier P, Pineau T, Lesca P. The 4S benzo(a)pyrene-binding protein is not a transcriptional activator of Cyp1a1 gene in Ah receptor-deficient (AHR−/−) transgenic mice. Arch Biochem Biophys 1998;349:349–55.

39. Bhat R, Wagner C, Bresnick E. The homodimic form of glycine N-methyl transferase acts as a polycyclic aromatic hydrocarbon-binding receptor. Biochem J 1997;36:9906–10.

40. Chang X, Roberts RJ. AdoMet-dependent methylation, DNA methyltransferases and base flipping. Nucleic Acids Res 2001;29:3784–95.